Solid-State Electrochemical Switch of Superconductor-Metal-Insulators

Xi Zhang[a*], Gowoon Kim[b], Qian Yang[b], Jiake Wei[c,d], Bin Feng[c], Yuichi Ikuhara[c,d] and Hiromichi Ohta[a*]

[a] *Research Institute for Electronic Science, Hokkaido University, N20W10, Kita, Sapporo 001-0020, Japan*

[b] *Graduate School of Information Science and Technology, Hokkaido University, N14W9, Kita, Sapporo 060-0814, Japan*

[c] *Institute of Engineering Innovation, The University of Tokyo, 2-11-16 Yayoi, Bunkyo, Tokyo 113-8656, Japan*

[d] *Elements Strategy Initiative for Structural Materials, Kyoto University, Yoshida-honmachi, Sakyo-ku, Kyoto 606-8501, Japan*

*Email: zhangxielle@gmail.com, hiromichi.ohta@es.hokudai.ac.jp

ABSTRACT: Controlling the oxygen content can manipulate the electrical conductivity of transition metal oxides (TMOs). Although the superconductor-metal-insulator transition is useful for functional devices, an electrical path must be developed to manipulate the oxygen deficiency (δ) while maintaining the solid-state. $YBa_2Cu_3O_{7-\delta}$ (YBCO, $0 \leqslant \delta \leqslant 1$) is a high transition temperature (T_c) TMO that can be modulated

from superconductor (T_c ~92 K when $\delta = 0$) to insulator ($\delta \sim 1$). Here, we show a simple and efficient way to manipulate δ in YBCO films using a solid-state electrochemical redox treatment. Applying a negative voltage injects oxide ions to the YBCO films, increasing T_c. Employing a positive voltage suppresses the superconducting transition and modulates the electrical conductivity. The present results demonstrate that the superconductor-metal-insulator transition of YBCO is modulated electrochemically in the solid state, opening possibilities of superconducting oxide-based device applications.

KEYWORDS: $YBa_2Cu_3O_{7-\delta}$, superconductor-metal-insulator transition, oxygen deficiency, electrochemical redox reaction, yttria-stabilized zirconia

INTRODUCTION

Various functional properties in transition metal oxides (TMOs) are strongly corelated with the valence state of the transition metal ions. Examples include the electrical conductivity, optical transmission, magnetism, and thermal conductivity. These properties can be manipulated by controlling the oxygen content[1].

Many methods have been proposed to control the oxygen content of TMOs, including heat treatment in a controlled oxidating/reducing atmosphere, heat treatment with a strong oxidating/ reducing agent[2], and electrochemical oxidation/reduction using liquid electrolyte[3]. Electrochemical methods are the most suitable to utilise the functional

properties of TMOs because reversible redox control of TMO-based devices is possible[4]. Additionally, an essential feature to realise reversible redox control of TMO-based electronic devices is a crystallographic similarity between the oxidised and reduced states. For example, the valence state of the cobalt ion in a $SrCoO_x$ oxygen sponge[5] can be adjusted electrochemically from +2 to +4[3, 6-10] due to the flexibility of the valence state of the cobalt ion and the topotactic change of the crystal lattice of $SrCoO_x$ between brownmillerite and perovskite.

In this study, we focus on the solid-state electrochemical redox treatment of $YBa_2Cu_3O_{7-\delta}$ (YBCO)[11]. YBCO is a well-known high-temperature superconductor. Its superconducting properties highly depend on the oxygen deficiency (δ)[12]. As δ varies from 1 to 0, YBCO ranges from metallic to semiconductive (**Fig. 1a**). The oxidised and reduced states have similar crystal structures. Additionally, the superconducting transition temperature (T_c) is strongly affected by δ. When δ is zero, T_c is ~92 K but T_c is almost 0 K when δ is ~0.6[12]. Therefore, controlled tuning of δ in YBCO is essential to develop superconducting oxide-based devices.

Similar to other TMOs, T_c of YBCO can be modulated in several ways such as (1) heat treatment in a controlled oxygen atmosphere[12], (2) electrostatic effect[13], (3) electrostatic effect plus an electrochemical reaction using an ionic liquid[14], and (4) an interfacial redox reaction via metal deposition[15]. However, these approaches have their limitation

for specific applications and face problems for device applications, where good repeatability is needed. In (1), the oxygen atmosphere must be precisely controlled, while the controllable sheet charge concentration in (2) is low. When employing the ionic liquid method, (3) suffers from a liquid leakage problem. In (4), the interfacial redox reaction is uncontrollable. In this light, the development of a simple and controllable method with easily accessible conditions is very important.

In this study, we demonstrate solid-state electrochemical switching of the superconductor-metal-insulator transition in a YBCO-based device, which efficiently manipulates δ in YBCO films. Applying a negative 10 V, the YBCO film shows an increased T_c from ~41 K to ~87 K, whereas applying a positive 10 V efficiently removes oxygen and successfully modulates the electrical conductivity of YBCO films from superconductor to insulator. The present results clearly show that the superconductor-metal-insulator transition of YBCO is modulated electrochemically in the solid state. Thus, this approach opens new possibilities of superconducting oxide-based device applications.

EXPERIMENTAL SECTION

Preparation of YBCO films: YBCO films (66 nm) were grown on (100) YSZ single crystal substates (10 mm × 10 mm × 0.5 mm) at 850 °C in an oxygen atmosphere (10 Pa) by the pulsed laser deposition technique (KrF excimer laser, ~2 J cm^{-2} $pulse^{-1}$, 10

Hz). Prior to the deposition of YBCO, an ~7-nm-thick layer of 8 mol% Gd-doped CeO_2 (GDC) was grown on the substrate at 750 °C under an oxygen pressure of 3 Pa.

Device fabrication and electrochemical redox reaction: Ag paint was pasted on the back side of the YSZ substrate as the gate electrode and Au foil was used as the counter electrode attached with the YBCO film (**Fig. 1b**). The electrochemical redox reaction was conducted at 300 °C with an applied voltage of +10 V for reduction and −10 V for oxidation. At 300 °C, the oxide ion conductivity of the YSZ substrate was ~3×10^{-6} S cm^{-1}. When +10 V was applied to the YSZ substrate, the oxide ion (O^{2-}) in the YBCO lattice was attracted by the positive bias through the YSZ substrate. This flow of O^{2-} ion was detected as the electronic current. On the other hand, when −10 V was applied to the YSZ substrate, O^{2-} ion in the air was injected to the YBCO film through the YSZ substrate by the negative bias. The oxygen deficiency δ of the $YBa_2Cu_3O_{7-\delta}$ films was modulated by applying different electron densities.

Crystallographic characterisation: Crystalline phase, orientation, and thickness of the resultant films were analysed by X-ray diffraction (XRD, Cu $K\alpha_1$, ATX-G, Rigaku). The atomic arrangement of the resultant films was visualized using STEM (ARM200CF, JEOL Co. Ltd) operated at 80 keV, to reduce the irradiation damage for YBCO. The convergence semi-angle is 24 mrad and the collection semi-angle span from 90 to 200 mrad for HAADF-STEM imaging. Further, the valence state of Cu was analysed by the

electron energy loss spectroscopy (EELS), which was recorded using an Enfina spectrometer (Gatan Inc.) with a cold-field emission gun. The collection semi-angle is 100 mrad and the dispersions used for collecting O K-edge and Cu L-edge are 0.1eV/channel and 0.25 eV/channel, respectively.

Resistivity and thermopower measurements: The electrical resistivities of the resultant YBCO films were measured by the dc four-probe method in the van der Pauw electrode configuration. In-Ga alloy was use as contact electrodes. The thermopower *S* of the YBCO films was measured using a steady-state method at room temperature. Our thermopower measurement setup is reported elesewhere.[16-17]

RESULTS AND DISCUSSION

Figure 1b schematically depicts the fabrication of a YBCO-based simple device. We chose an yttria-stabilized zirconia (YSZ) single crystal as the substrate because YSZ is a well-known oxide ion conducting solid electrolyte and YBCO can be heteroepitaxially grown on YSZ. YBCO films (66 nm) were heteroepitaxially grown on 8 mol% Gd-doped CeO_2 (7 nm) buffered YSZ substrate by the pulsed laser deposition (PLD) method. After YBCO film growth, Ag paint was pasted on the back side of the YSZ substrate. Then the YBCO film surface was mechanically attached on Au foil. Finally, the electrochemical redox treatments were performed at 300 °C in air.

We applied voltages of +10 V for reduction and −10 V for oxidation. The applied electron density (Q) was calculated as $Q = (I \cdot t \cdot e^{-1} \cdot v^{-1})$, where I, t, e, and v are the applied current, time, electron charge, and film volume, respectively. As summarised in **Fig, 1c**, we oxidised three samples as (B) $Q = -2.93 \times 10^{22}$ cm^{-3}, (C) -1.01×10^{23} cm^{-3}, and (D) -1.32×10^{23} cm^{-3}, and we reduced four samples as (E) $+2.5 \times 10^{21}$ cm^{-3}, (F) 4.0×10^{21} cm^{-3}, (G) 8.9×10^{21} cm^{-3}, and (H) 9.4×10^{21} cm^{-3}. Sample A was kept in the as-grown state for comparison.

Figure 2a shows the temperature dependence of electrical resistivity ($\rho-T$ curves) of samples A−H. The $\rho-T$ curves change drastically as Q is varied. The as-grown sample (A) and oxidised samples (B, C, and D) show clear superconducting transitions. By increasing Q, samples show a higher T_c and a lower normal-state resistivity. **Figure 2b** plots the normalised resistivity at 100 K ($\rho/\rho_{100\,K}$) of samples A, B, C, and D as a function of temperature. T_c significantly increases from ~41 K (A) to ~87 K (D) after applying Q of -1.32×10^{23} cm^{-3} (**Fig. 2c**). In contrast, the superconducting transition is completely suppressed by applying a positive voltage without an apparent transition down to the lowest measured temperature (samples E, F, G, and H). Additionally, the normal-state resistivity of the reduced samples increases with the reduction degree. These results clearly indicate that a solid-state electrochemical switch of superconductor-metal-insulator is realised.

It should be noted that T_c of the as-grown sample is lower than that of $YBa_2Cu_3O_7$ (T_c ~92 K), which is usually obtained by post-annealing in an oxygen atmosphere, indicating that the oxidised sample D (T_c ~87 K) is oxygen deficient. To clarify δ in the YBCO films, we analysed the crystal lattice of the YBCO films using high-resolution X-ray diffraction (XRD, Cu $K\alpha_1$) (**Fig. S2**). Only intense 00*l* (*l* = integer) YBCO peaks are seen in the out-of-plane XRD patterns together with 002 GDC/YSZ in the out-of-plane XRD patterns (**Fig. S2a**). The full-width at half maximum (FWHM) of the out-of-plane X-ray rocking curves (data not shown) is narrower than 0.1°, indicating films with a strong *c*-axis orientation. In the in-plane Bragg diffraction patterns, intense diffraction peaks of *h*00 YBCO are seen together with 110 YSZ (**Fig. S2c**). Four-fold symmetry (data not shown) is clearly observed, indicating heteroepitaxial growth and a stabilised tetragonal structure. These results reveal that the epitaxial relationship between the YBCO films and the substrate is (001)[100] YBCO || (001)[110] GDC/YSZ. The redox treatment does not affect the peak position of *h*00 (*h* = 1 and 2) YBCO in the in-plane Bragg diffraction patterns (**Fig. S2c**). This suggests that the *a*-axis lattice parameter (0.3860 nm) is constant, which is consistent with that of tetragonal $YBa_2Cu_3O_{7-\delta}$[12]. The peaks in the out-of-plane Bragg diffraction patterns clearly shift (**Fig. S2b**).

Table S1 lists the extracted *c*-axis lattice parameters of the YBCO films. Although the literature indicates a clear relationship between the lattice parameter-oxygen content and T_c[12], the extracted *c*-axis lattice parameter does not reproduce the observed T_c. This is

probably due to the in-plane lattice strain originating from the GDC/YSZ substrate.

To clarify the oxygen content in the YBCO films, we measured thermopower (S) of the YBCO films at room temperature (**Table S1**) because S is an excellent measure to analyse the Fermi energy location of a material. We obtained the oxygen content (**Table S1**) using the following equation, which was extracted from the data reported by Cochrane *et al*.[18] in 1994

$$\delta = -0.8120 \exp(-S / 72.244) + 0.8992$$

Figure 3a shows the calibration curve of δ, which is obtained from the reported $S - \delta$ data. Using the thermopower data and the calibration curve, we determined the δ values of samples A − H. **Figure 3b** plots the change in the electrical resistivity (ρ) as a function of δ. The ρ values increase exponentially with increasing δ. Although the observed ρ values are slightly higher than the reported values[19], the overall increasing tendency looks similar. **Figure 3c** shows the *c*-axis lattice parameter. The *c*-axis lattice parameter of the present $YBa_2Cu_3O_{7-\delta}$ films is ~0.01 nm longer than the reported values[12]. **Figure 3d** shows T_c of the samples A, B, and D. Compared to the reported values[12], the observed T_c of the present $YBa_2Cu_3O_{7-\delta}$ films is ~5 K lower. These results reveal that the solid-state electrochemical redox treatments modulate δ in $YBa_2Cu_3O_{7-\delta}$ films in the range of $\sim 0 \leqslant \delta \leqslant \sim 0.87$.

To further clarify the crystallographic change after the electrochemical reduction and

oxidation treatment, we performed high-angle annular dark-field scanning transmission electron microscopy (HAADF-STEM) observations of samples D (oxidised) and H (reduced) (**Fig. 4**). A layered crystal structure of $YBa_2Cu_3O_{7-\delta}$ films is clearly visualized together with ~10-nm-thick GDC/YSZ substrate in both samples (**Figs. 4a and 4c**). Similar to previous observations of oxidised YBCO films[20-21], many planar defects are also detected in the HAADF-STEM image of sample D. The crystal lattices of sample H (**Fig. 4b**) and sample D (**Fig. 4d**) agree well with the crystal structure models of $YBa_2Cu_3O_6$ and $YBa_2Cu_3O_7$ (**Fig. 1a**). Thus, the similar crystal structures of $YBa_2Cu_3O_6$ and $YBa_2Cu_3O_7$ allow δ to be modulated by solid-state electrochemical redox treatments.

The valence state change of the Cu ion in the chain structure of $YBa_2Cu_3O_{7-\delta}$ was also visualized by electron energy loss spectroscopy (EELS). Although the Cu L-edge spectra of the planes do not differ significantly by the oxidation states (**Fig. 4e**), the Cu^{2+} intensity of chains[22] in the oxidised film is stronger than that of the reduced one (**Fig. 4f**). Additionally, the O K-edge spectra of the films do not differ significantly (**Figs. 4g** and **4h**). Although Gauquelin *et al.*[22] detected an extra EELS peak at ~529 eV in the chains of $YBa_2Cu_3O_7$ single crystal, our sample do not show an extra peak. Since the O K-edge is sensitive to the crystal symmetry, one possible explanation of this difference is that the crystal symmetry of our $YBa_2Cu_3O_{7-\delta}$ samples is always tetragonal whereas the $YBa_2Cu_3O_{7-\delta}$ single crystal undergoes a symmetry change from tetragonal

around δ ~0.65 (orthorhombic :0 $\leqslant$ δ $\leqslant$ 0.65, tetragonal: 0.65 < δ < 1)[12]. Thus, the solid-state electrochemical redox treatments successfully induces a topotactic redox reaction in the chain part of the $YBa_2Cu_3O_{7-\delta}$ crystal.

Here, we discuss the possibility of reducing the operating temperature. When the operating temperature is reduced, the oxide ion (O^{2-}) conductivity of YSZ is exponentially reduced[23]. Thus, the redox treatment requires a longer time and a higher voltage. In the present work, we used a 0.5-mm-thick YSZ single crystal as the substrate. One solution would be to use a thinner YSZ single crystal substrate or thin film.

Another important factor toward device applications is cyclability. We confirmed a good cyclability of the superconductor-metal-insulator modulation by repeating the electrochemical redox treatment for 5 cycles (**Figure S3**). The present method repeatedly modulates the electrical resistivity and lattice parameter (**Figures S4−S6**). This crystallographic stability originates from the similar crystal structures of the oxidized and reduced states. The present results clearly demonstrate that the superconductor-metal-insulator transition of YBCO is modulated electrochemically in the solid state.

CONCLUSIONS

In summary, we demonstrated a YBCO-based functional device that controls the superconductor-metal-insulator transition by solid-state electrochemical redox treatments. The device is simple and composed of YBCO/GDC/YSZ layers. Applying a negative voltage to the YBCO films injects oxide ions into the YBCO films, increasing T_c. Employing a positive voltage completely suppresses the superconducting transition. Hence, the results show that the electrical conductivity is well modulated electrochemically in the solid state. Consequently, this study opens new possibilities of superconducting oxide-based device applications.

ASSOCIATED CONTENT

Supporting Information

Supporting Information is available free of charge via the Internet at https://pubs.acs.org/doi/10.1021/acsami.XXXXXXX.

Oxygen deficiency (δ), electron density (Q), lattice parameter (c), thermopower (S) at room temperature, electrical resistivity (ρ) at room temperature, and superconducting transition temperature (T_c) of the YBCO samples; Applied current densities for the electrochemical redox treatment; X-ray diffraction patterns of the $YBa_2Cu_3O_{7-\delta}$ films with various redox states; Applied current densities for the electrochemical redox treatment; X-ray diffraction patterns of the $YBa_2Cu_3O_{7-\delta}$ films after cycling electrochemical oxidation and reduction; c-axis lattice parameter changes after cycling electrochemical oxidation and reduction; $\rho-T$ curves of the $YBa_2Cu_3O_{7-\delta}$ films after different oxidation-reduction cycles.

AUTHOR INFORMATION

Corresponding Authors

Xi Zhang − Research Institute for Electronic Science, Hokkaido University, N20W10, Kita, Sapporo 001-0020, Japan

ORCiD: orcid.org/0000-0001-9389-5082

Email: zhangxielle@gmail.com

Hiromichi Ohta − Research Institute for Electronic Science, Hokkaido University, N20W10, Kita, Sapporo 001-0020, Japan

ORCiD: orcid.org/0000-0001-7013-0343

Email: hiromichi.ohta@es.hokudai.ac.jp

Author

Gowoon Kim − Graduate School of Information Science and Technology, Hokkaido University, N14W9, Kita, Sapporo 060-0814, Japan

ORCiD: orcid.org/0000-0002-5803-839X

Qian Yang − Graduate School of Information Science and Technology, Hokkaido University, N14W9, Kita, Sapporo 060-0814, Japan

ORCiD: orcid.org/0000-0002-1916-7025

Jiake Wei − Elements Strategy Initiative for Structural Materials, Kyoto University, Yoshida-honmachi, Sakyo-ku, Kyoto 606-8501, Japan

ORCiD: orcid.org/0000-0001-7450-7005

Bin Feng − Institute of Engineering Innovation, The University of Tokyo, 2−11−16 Yayoi, Bunkyo, Tokyo 113-8656, Japan

ORCiD: orcid.org/0000-0002-4306-2979

Yuichi Ikuhara − Institute of Engineering Innovation, The University of Tokyo, 2−11−16 Yayoi, Bunkyo, Tokyo 113−8656, Japan

ORCiD: orcid.org/0000-0003-3886-005X

Author Contributions

X.Z., G.K., Q.Y., and H.O. prepared the samples and conducted the measurements. J.W, B.F, and Y.I. performed STEM and EELS analyses. X.Z. and H.O. planned and supervised the project. All authors discussed the results and commented on the manuscript.

Funding Sources

Gowoon Kim received funding from Grants-in-Aid for JSPS Fellows (2010147550).

Qian Yang received funding from Grants-in-Aid for JSPS Fellows (21J10042).

Bin Feng received founding from Grants-in-Aid of the JSPS (19H05791).

Hiromichi Ohta received founding from Grants-in-Aid of the JSPS (19H05788).

Notes

The authors declare no competing financial interest.

ACKNOWLEDGEMENTS

This research was supported by Grants-in-Aid for Innovative Areas (19H05791 and 19H05788) from the Japan Society for the Promotion of Science (JSPS). Part of this work was supported by the Dynamic Alliance for Open Innovation Bridging Human, Environment, and Materials, and by the Network Joint Research Center for Materials and Devices. G.K. and Q.Y. were supported by Grants-in-Aid for JSPS Fellows (2010147550, 21J10042). Part of this work was conducted at the Advanced Characterization Nanotechnology Platform of The University of Tokyo, supported by "Nanotechnology Platform" of the Ministry of Education, Culture, Sports, Science and Technology (MEXT), Japan (JPMXP09A21UT0161).

REFERENCES

1. Kalinin, S. V.; Spaldin, N. A., Functional Ion Defects in Transition Metal Oxides. *Science* **2013,** *341*, 858-859.

2. Tsujimoto, Y.; Tassel, C.; Hayashi, N.; Watanabe, T.; Kageyama, H.; Yoshimura, K.; Takano, M.; Ceretti, M.; Ritter, C.; Paulus, W., Infinite-layer iron oxide with a square-planar coordination. *Nature* **2007,** *450*, 1062-1065.

3. Lu, N. P.; Zhang, P. F.; Zhang, Q. H.; Qiao, R. M.; He, Q.; Li, H. B.; Wang, Y. J.; Guo, J. W.; Zhang, D.; Duan, Z.; Li, Z. L.; Wang, M.; Yang, S. Z.; Yan, M. Z.; Arenholz, E.; Zhou, S. Y.; Yang, W. L.; Gu, L.; Nan, C. W.; Wu, J.; Tokura, Y.; Yu, P., Electric-field control of tri-state phase transformation with a selective dual-ion switch. *Nature* **2017,** *546*, 124.

4. Leighton, C., Electrolyte-based ionic control of functional oxides. *Nature Mater.* **2019,** *18*, 13-18.

5. Jeen, H.; Choi, W. S.; Biegalski, M. D.; Folkman, C. M.; Tung, I. C.; Fong, D. D.; Freeland, J. W.; Shin, D.; Ohta, H.; Chisholm, M. F.; Lee, H. N., Reversible redox reactions in an epitaxially stabilized $SrCoO_x$ oxygen sponge. *Nature Mater.* **2013,** *12*, 1057-1063.

6. Nemudry, A.; Rudolf, P.; Schollhorn, R., Topotactic electrochemical redox reactions of the defect perovskite $SrCoO_{2.5+x}$. *Chem. Mater.* **1996,** *8*, 2232-2238.

7. Katase, T.; Suzuki, Y.; Ohta, H., Reversibly switchable electromagnetic device with leakage-free electrolyte. *Adv. Electron. Mater.* **2016,** *2*, 1600044.

8. Lu, Q. Y.; Yildiz, B., Voltage-Controlled Topotactic Phase Transition in Thin-Film $SrCoO_x$ Monitored by In Situ X-ray Diffraction. *Nano Lett.* **2016,** *16*, 1186-1193.

9. Yang, Q.; Cho, H. J.; Jeen, H.; Ohta, H., Macroscopic visualization of fast electrochemical reaction of $SrCoO_x$ oxygen sponge. *Adv. Mater. Interfaces* **2019,** *6*, 1901260.

10. Lu, Q. Y.; Huberman, S.; Zhang, H. T.; Song, Q. C.; Wang, J. Y.; Vardar, G.; Hunt, A.; Waluyo, I.; Chen, G.; Yildiz, B., Bi-directional tuning of thermal transport in $SrCoO_x$ with electrochemically induced phase transitions. *Nature Mater.* **2020,** *19*, 655-664.

11. Wu, M. K.; Ashburn, J. R.; Torng, C. J.; Hor, P. H.; Meng, R. L.; Gao, L.; Huang, Z. J.; Wang, Y. Q.; Chu, C. W., Superconductivity at 93 K in a new mixed-phase Y-Ba-Cu-O compound system at ambient pressure. *Phys. Rev. Lett.* **1987,** *58*, 908-910.

12. Jorgensen, J. D.; Veal, B. W.; Paulikas, A. P.; Nowicki, L. J.; Crabtree, G. W.;

Claus, H.; Kwok, W. K., Structural-Properties of Oxygen-Deficient $YBa_2Cu_3O_{7-\delta}$. *Phys. Rev. B* **1990,** *41*, 1863-1877.

13. Leng, X.; Garcia-Barriocanal, J.; Bose, S.; Lee, Y.; Goldman, A. M., Electrostatic Control of the Evolution from a Superconducting Phase to an Insulating Phase in Ultrathin $YBa_2Cu_3O_{7-x}$ Films. *Phys. Rev. Lett.* **2011,** *107*, 027001.

14. Perez-Munoz, A. M.; Schio, P.; Poloni, R.; Fernandez-Martinez, A.; Rivera-Calzada, A.; Cezar, J. C.; Salas-Colera, E.; Castro, G. R.; Kinney, J.; Leon, C.; Santamaria, J.; Garcia-Barriocanal, J.; Goldman, A. M., In operando evidence of deoxygenation in ionic liquid gating of $YBa_2Cu_3O_{7-x}$. *Proc. Natl. Acad. Sci. USA* **2017,** *114*, 215-220.

15. Murray, P. D.; Gilbert, D. A.; Grutter, A. J.; Kirby, B. J.; Hernandez-Maldonado, D.; Varela, M.; Brubaker, Z. E.; Liyanage, W. L. N. C.; Chopdekar, R. V.; Taufour, V.; Zieve, R. J.; Jeffries, J. R.; Arenholz, E.; Takamura, Y.; Borchers, J. A.; Liu, K., Interfacial-Redox-Induced Tuning of Superconductivity in $YBa_2Cu_3O_{7-\delta}$. *ACS Appl. Mater. Interfaces* **2020,** *12*, 4741-4748.

16. Ohta, H.; Sato, Y.; Kato, T.; Kim, S.; Nomura, K.; Ikuhara, Y.; Hosono, H., Field-induced water electrolysis switches an oxide semiconductor from an insulator to a metal. *Nature Commun.* **2010,** *1*, 118.

17. Ohta, H.; Mizuno, T.; Zheng, S.; Kato, T.; Ikuhara, Y.; Abe, K.; Kumomi, H.; Nomura, K.; Hosono, H., Unusually Large Enhancement of Thermopower in an Electric Field Induced Two‐Dimensional Electron Gas. *Adv. Mater.* **2012,** *24*, 740-744.

18. Cochrane, J. W.; Russell, G. J.; Matthews, D. N., Seebeck Coefficient as an Indicator of Oxygen-Content in YBCO. *Phys. C* **1994,** *232*, 89-92.

19. Arias, D.; Sefrioui, Z.; Loos, G. D.; Agullo-Rueda, F.; Garcia-Barriocanal, J.; Leon, C.; Santamaria, J., Pair breaking by chain oxygen disorder in light-ion irradiated $YBa_2Cu_3O_x$ thin films. *Phys. Rev. B* **2003,** *68*, 094515.

20. Gauquelin, N.; Zhang, H.; Zhu, G. Z.; Wei, J. Y. T.; Botton, G. A., Atomic-scale

identification of novel planar defect phases in heteroepitaxial $YBa_2Cu_3O_{7-\delta}$ thin films. *AIP Adv.* **2018,** *8*, 055022.

21. Mundet, B.; Hartman, S. T. T.; Guzman, R.; Idrobo, J. C. C.; Obradors, X.; Puig, T.; Mishra, R.; Gazquez, J., Local strain-driven migration of oxygen vacancies to apical sites in $YBa_2Cu_3O_{7-x}$. *Nanoscale* **2020,** *12*, 5922-5931.

22. Gauquelin, N.; Hawthorn, D. G.; Sawatzky, G. A.; Liang, R. X.; Bonn, D. A.; Hardy, W. N.; Botton, G. A., Atomic scale real-space mapping of holes in $YBa_2Cu_3O_{6+\delta}$. *Nature Commun.* **2014,** *5*, 4275.

23. Manning, P. S.; Sirman, J. D.; DeSouza, R. A.; Kilner, J. A., The kinetics of oxygen transport in 9.5 mol % single crystal yttria stabilised zirconia. *Solid State Ionics* **1997,** *100*, 1-10.

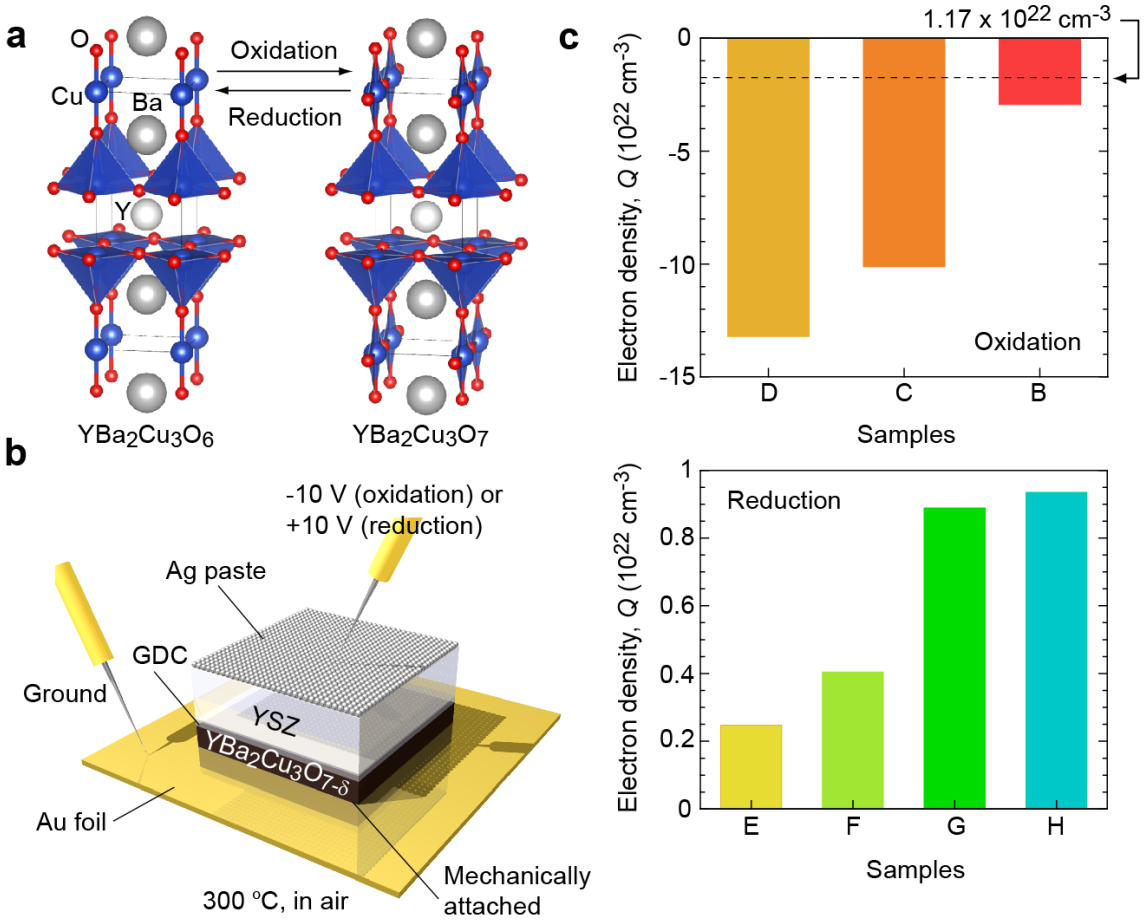

Figure 1. Solid-state electrochemical switching of superconductor-metal-insulator of $YBa_2Cu_3O_{7-\delta}$ films. (a) Schematic of the crystal structure of $YBa_2Cu_3O_6$ (insulator) and $YBa_2Cu_3O_7$ (high-T_c superconductor). Crystal structures are similar. (b) Schematic illustration of a solid-state electrochemical switch. $YBa_2Cu_3O_{7-\delta}$ film, which is grown on a GDC-buffered YSZ substrate, is mechanically attached on Au foil. Ag paint is pasted on the back side of YSZ substrate. Negative (positive) 10 V is applied at 300 °C in air for oxidation (reduction) of the $YBa_2Cu_3O_{7-\delta}$ film. (c) Electron density (Q) applied to $YBa_2Cu_3O_{7-\delta}$ films during the electrochemical redox treatment.

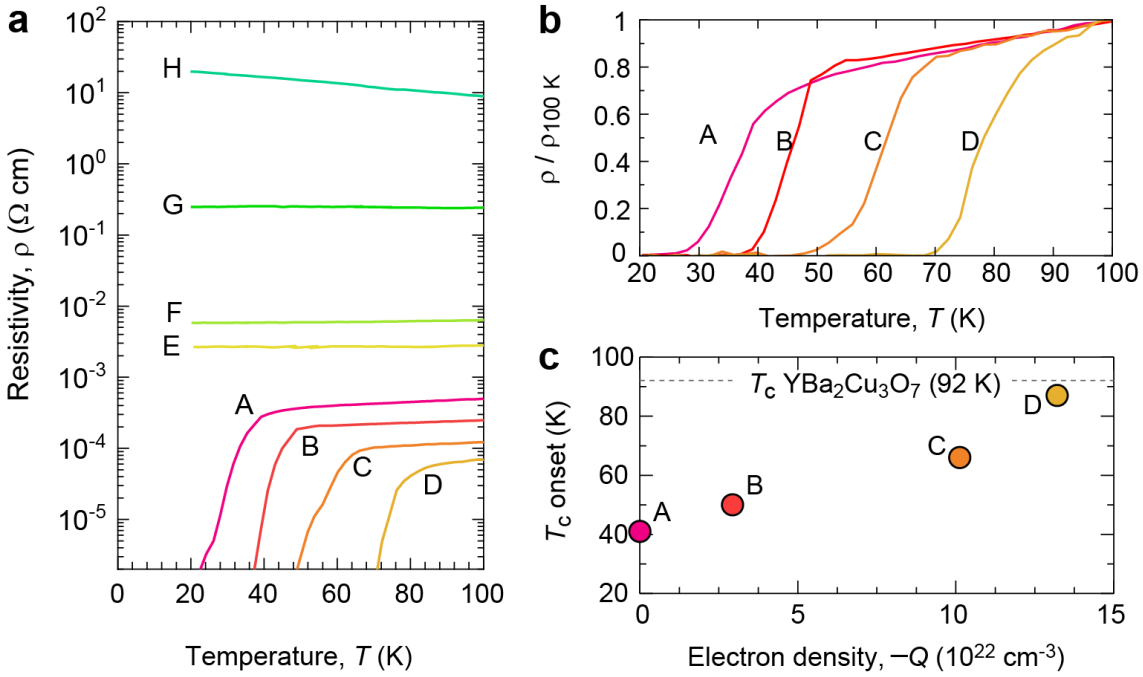

Figure 2. Superconductor-metal-insulator modulation of $YBa_2Cu_3O_{7-\delta}$ films by the solid-state electrochemical redox treatments. (a) $\rho-T$ curves of the $YBa_2Cu_3O_{7-\delta}$ films with various redox states. (b) Normalised resistivity of samples A, B, C, and D. (c) Superconducting transition temperature (T_c onset) as a function of electron density (Q). T_c onset gradually increases and approaches the that of $YBa_2Cu_3O_7$ (92 K).

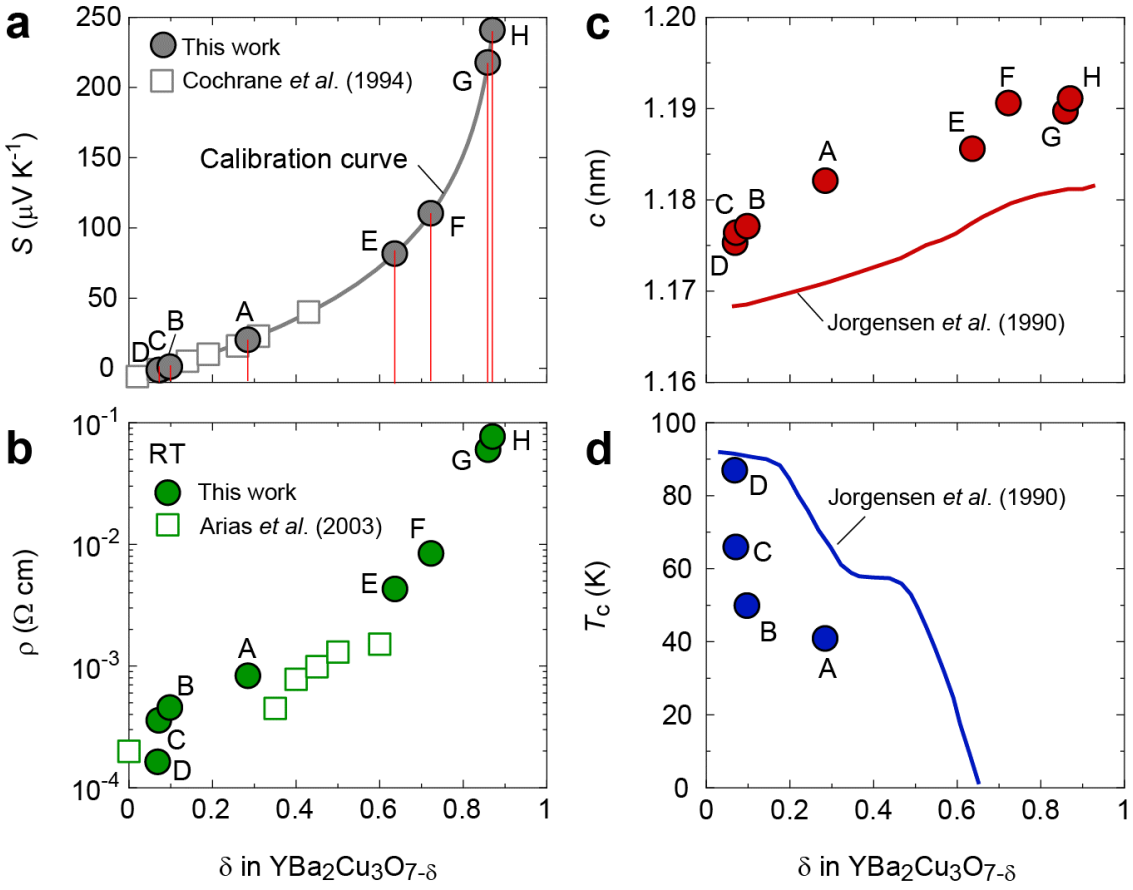

Figure 3. Solid-state electrochemical modulation of the electron deficiency (δ) in the $YBa_2Cu_3O_{7-\delta}$ films. (a) Thermopower (S). Calibration curve of δ in $YBa_2Cu_3O_{7-\delta}$ is from the reported S–δ data. δ values of the present films are determined using the calibration curve. (b) Change in the electrical resistivity (ρ) as a function of δ. Several reported values are plotted for comparison. (c) c-Axis lattice parameter. c-Axis lattice parameter of the present $YBa_2Cu_3O_{7-\delta}$ films is ~0.01 nm longer than the reported values. (d) Superconducting transition temperature (T_c). Compared to the reported values, T_c of the present $YBa_2Cu_3O_{7-\delta}$ films is ~5 K lower.

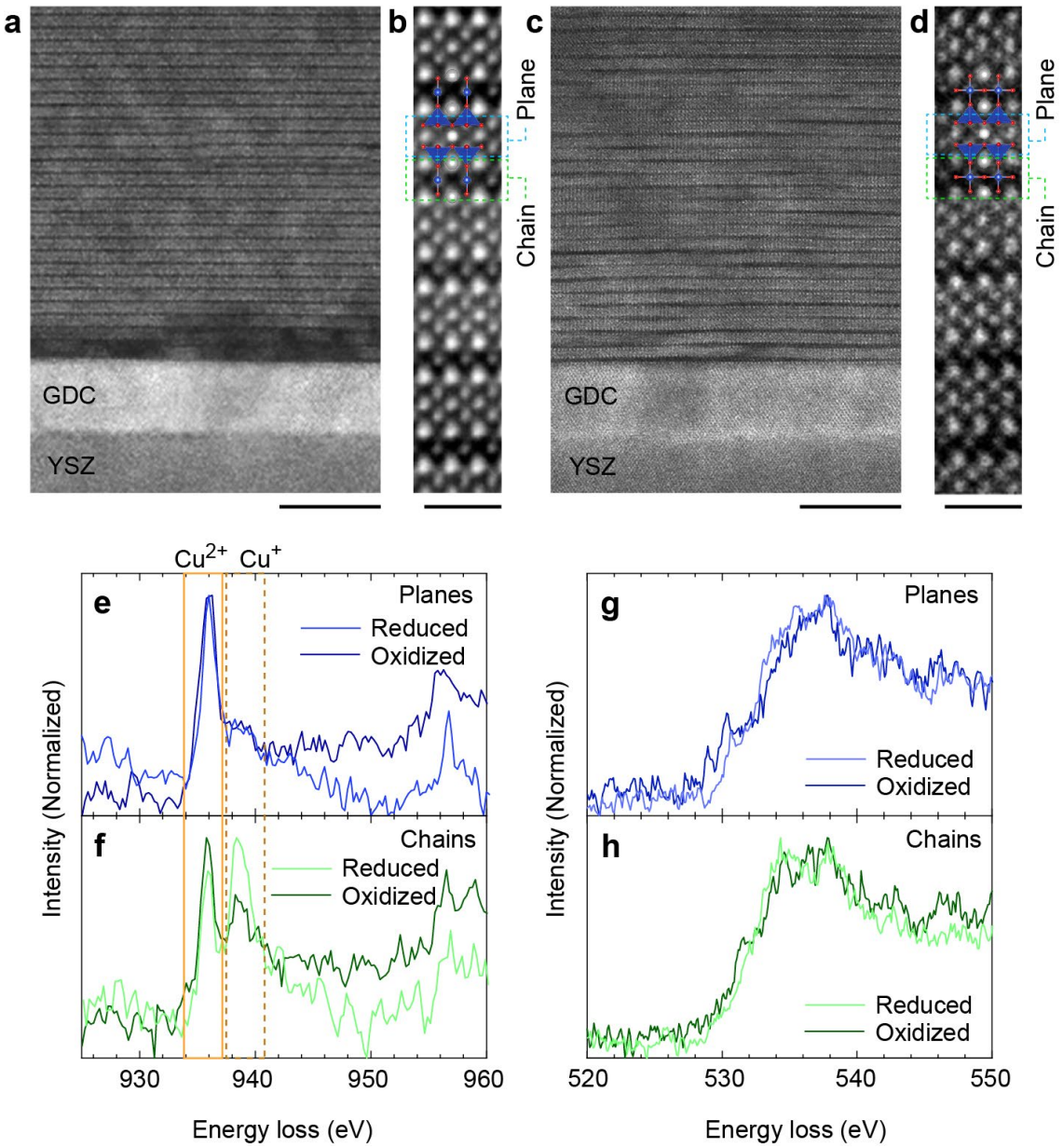

Figure 4. Microstructure and valence states of the $YBa_2Cu_3O_{7-\delta}$ films. HAADF-STEM images of (a) reduced (H) and (c) oxidized (D) $YBa_2Cu_3O_{7-\delta}$ films. Layers of $YBa_2Cu_3O_{7-\delta}$, GDC, and YSZ are clearly visualized. (b, c) Magnified HAADF-STEM images. Scale bars are (a, c) 10 nm and (b, d) 1 nm. (e–h) EELS spectra of the $YBa_2Cu_3O_{7-\delta}$ films. Cu L-edge spectra of planes do not significantly differ by oxidation state. On the other hand, the Cu^{2+} intensity of chains in the oxidized film is stronger than that of the reduced one. (g, h) No significant difference is detected around the O K-edge spectra of the films.

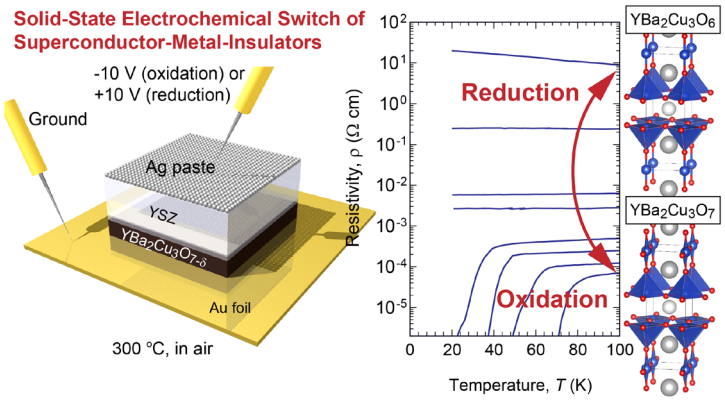
Solid-State Electrochemical Switch of
Superconductor-Metal-Insulators
-10 V (oxidation) or
+10 V (reduction)
Ground
Ag paste
YSZ
YBa2Cu3O7-δ
Au foil
300 °C, in air
Resistivity, ρ (Ω cm)
Reduction
Oxidation
Temperature, T (K)
YBa2Cu3O6
YBa2Cu3O7

TOC Figure